ACS OMEGA

http://pubs.acs.org/journal/acsodf

Article

# Binding Mechanisms Between Laser-Welded Polyamide-6.6 and Native Aluminum Oxide

Pierre Hirchenhahn, Adham Al-Sayyad, Julien Bardon, Peter Plapper, and Laurent Houssiau*

Cite This: *ACS Omega* 2021, 6, 33482−33497

Read Online

ACCESS | Metrics & More | Article Recommendations | Supporting Information

**ABSTRACT:** Nowadays, hybrid polymer/metal assemblies experience a growing demand in the industry, especially for transports and biomedical purposes. Those assemblies offer many advantages, such as lightweight structures and corrosion resistance. The main difficulty to assemble them remains. In this sense, laser welding is more than a promising technique because of its rapidity, the absence of intermediate materials, and its high design freedom. Unfortunately, several fundamental aspects are not well understood yet, as the chemical bonding at the interface. For this work, common materials are studied: polyamide-6.6 and aluminum. A previous published work strongly suggests the formation of a C−O−Al bond at the interface, but this information needs to be confirmed and the reaction mechanism is still uncertain. To achieve this goal, two different model samples were prepared. The first ones are spin-coated layers of polyamide-6.6 on mirror polished aluminum; the other samples are made of a layer of *N*-methylformamide mimicking the reactive part of the polymer, dip-coated on aluminum. Both sample types were analyzed with XPS and ToF-SIMS and display similar results: C−O−Al bond formation at the interface is confirmed and a reaction mechanism is proposed.

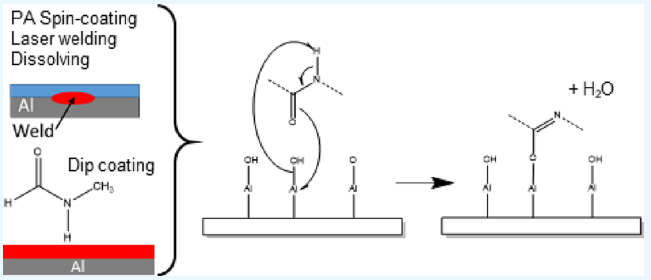


## 1. INTRODUCTION

To comply with the environmental objectives set with the Paris agreement on climate change in 2015, the interest for polymer/metal hybrid systems is increasing in several industrial sectors, especially for automotive or aerospace applications. Even if there are many promising possibilities with these hybrid assemblies, there are still many challenges to overcome. One of these challenges is the way of assembling the dissimilar materials. Three main possibilities exist nowadays: mechanical fastening,[1] adhesive bonding,[2,3] and welding.[3−5] The main drawback of mechanical fastening is that weight reduction is not optimum and these assemblies present low fatigue and corrosion resistance. Adhesive bonding needs several time and energy consuming preparations and curing steps and is often associated with the use of harmful chemicals. In order to face at best the environmental challenges ahead, the use of welding techniques to assemble metal with polymers appears as the best way.

Among welding techniques, laser welding is catching more and more attention. Indeed, laser welding presents many advantages for industrial use: quickness, high reproducibility, and more importantly, high design freedom. In addition, the laser welding process can be easily automated, which explains its high reproducibility. The high design freedom concerns the different size possibilities, tiny or large parts, and their shape, flat or round. The spatial flexibility and high precision of the laser beam allow it to create miniaturized weld seams of complex geometries. Another interesting point is that laser welding does not require additional materials than the ones to be welded like for adhesive bonding. Several articles relate the possibility to tune the adhesion strength by performing different surface pretreatments.[6−8] Nonetheless, laser welding remains expensive to implement in a production line.[3−5]

The basic principle of laser welding is to irradiate a laser beam on the materials, which will bring enough energy, transformed into heat, to weld them. Two different welding configurations[3,5] exist: direct and indirect welding. Direct welding[9−11] consists of irradiating the laser beam through the polymer to reach the interface of the materials. Historically, this configuration was applied in the first example of polymer−metal laser welding, in the pioneering work of Katayama and Kawahito in 2008.[10] The beam is absorbed at the interface by the metal as heat, which will melt the thermoplastic polymer and thereby forming the weld. The main restriction of this configuration is that the polymer must be transparent to the laser, which limits the choice of weldable polymers. In indirect welding[3,5,7,9] (or heat conduction joining) the laser beam is irradiated on the metal. The energy absorbed is also converted

Received: August 9, 2021
Accepted: November 2, 2021
Published: December 3, 2021

into heat, which is not created at the interface but is conducted from the metal surface to the polymer−metal interface. The thermoplastic polymer also melts and the two materials are welded. Here, the choice of weldable polymer is broader than for direct welding, which is why indirect laser welding was privileged in this study. Over the years, several material combinations were tested and showed the great versatility of the technique.[9,12,13] As mentioned above, different surface pretreatments prior to welding were also tested in order to tune the joint mechanical resistance.[6−8] More fundamental work on laser welding is quite scarce. Schricker *et al.*[14,15] studied the impact of polymer melting and further recrystallization on the weld mechanical resistance. Lamberti *et al.*[7] investigated the role of the aluminum−polyamide interface temperature and input laser power and showed that a very low power does not allow to get a good weld, while a very high power leads to polymer degradation, certainly because the corresponding interface temperature is too high. The optimum temperature is slightly above the polymer melting temperature. This is completed by the work on interfacial heat transfer done by Al Sayyad *et al.*,[16] which also allowed to better understand the impact of surface pretreatment, both on surface properties and thermal contact resistance of the interface. The existence of a chemical bond at the interface between laser-welded polyamide-6.6 and aluminum was investigated in a previous article.[17] In this article, a method to access and analyze the buried interface of aluminum−polyamide-welded assemblies was developed. Results show the existence of a C−O−Al bond at the interface, but a reaction with nitrogen forming a C−N−Al bond could not be completely excluded. Moreover, the results did not allow obtaining any conclusion on the reactivity of the metal, leaving the question of the reaction mechanism between both materials open. These are the objectives of the current article: (1) clarifying the existence or not of C−N−Al bonds and (2) investigating the reactivity of the metal, which will lead to a conclusion on the reaction mechanism.

## 2. RESULTS AND DISCUSSION

**2.1. Spin-Coated Samples.** *2.1.1. Surface Composition.* The surface elemental composition measured with XPS is presented in Table 1. The nitrogen percentage increases from the reference samples (3.7%) to the weld zone (4.7%), while the out of weld (4.4%) has an intermediate percentage. It is noticeable that the nitrogen percentage in the reference is more than four times higher than on a simple aluminum surface (of the same alloy and after mirror polishing). The oxygen percentage decreases from 42.3 to 37.6% from the reference to the weld. These two changes are caused by the presence of a polyamide-6.6 thin film on the surface in the weld, which is obviously the source of nitrogen but contains less oxygen than an aluminum oxide surface (12.5% in PA-6.6 against 60% in pure $Al_2O_3$). The thin film of polyamide-6.6 is thinner than the depth of analysis of XPS, so that not only the polymer is detected in XPS but also the aluminum surface underneath, which explains why the percentages of the different elements present intermediate values between the aluminum surface and pure polyamide-6.6. The average carbon percentage from the reference to the weld seems to be slightly increasing in the weld. The average percentage of aluminum decreases from the reference to the weld and is even lower in the out of weld, but as for the carbon percentage, the standard deviations of each zone overlap each other. These results indicate that some polyamides are still adsorbed in the reference, the out of weld, and in the weld after dissolution with 2,2,2-trifuoroethanol but not in the same amount. The spin-coating process allows the polyamide-6.6 to adsorb on the surface, and the welding increases the amount of polymer "sticking" in the weld to amounts comparable to previously published results on broken assemblies.[17] Interestingly, no fluorine is detected, which suggests that the solvent used for dissolution—2,2,2-trifluoroethanol—does not adsorb on the surface. Hence, it does not alter the surface analysis, as observed previously.[17]

**Table 1. XPS Average Elemental Composition and its Standard Deviation of an Aluminum Surface, in the Reference, out of the Weld, and in the Weld, and the Theoretical Elemental Composition of Polyamide-6.6 (PA-6.6)**

| sample | % O | % Al | % C | % N |
|---|---|---|---|---|
| Al surface | 42.2 (±1.5) | 27.3 (±1.8) | 29.7 (±2.7) | 0.8 (±0.4) |
| Ref | 42.3 (± 1.3) | 27.1 (±2.5) | 27.0 (±3.2) | 3.7 (±0.5) |
| out of weld | 39.8 (±0.9) | 24.4 (±1.2) | 31.5 (±1.8) | 4.4 (±0.3) |
| weld | 37.6 (±0.9) | 25.7 (±1.3) | 32.0 (±1.9) | 4.7 (±0.3) |
| PA-6.6 theory | 12.5 | | 75 | 12.5 |

Figure 1a−c shows the high-resolution spectra of the C 1s regions in the reference, out of the weld, and in the weld. First, a C−C/C−H contribution was attributed at 284.8 eV for each spectrum, which served as a calibration peak. Then, a C−O/C−N contribution was found around 285.8 eV. At last, a contribution of C═O around 287.9 eV was added. The calculation of the ratio of the C−O/C−N contribution to the C═O one gives a similar result for all the samples: 1.2 (±0.2) for the reference, 1.3 (±0.3) for the out of the weld, and 1.1 (±0.1) in the weld. All the spectra of carbon C 1s can be interpreted with the characteristic peaks of polyamide-6.6.[18−21] This is supported by the spectra from the N 1s region shown in Figure 1d−f, where an amide peak can be identified around 399.8 eV.[22−24] It is the only contribution clearly identified. The O 1s regions of the reference, the out of weld, and in the weld are depicted in Figure 1g−i. Three contributions were identified: one for the aluminum oxide at 531.4 eV, one for the aluminum hydroxide at 532.3 eV, and one for organic molecules, in this case, polyamide and water at 533.2 eV.[22,25,26] The Al 2p region presented in Figure 1j−l, is fitted using three contributions: one for Al $2p_{3/2}$ at 72.4 eV, one for Al $2p_{1/2}$ at 72.8 eV, which are characteristic for metallic aluminum, and the last broad contribution at 74.5 eV corresponds to oxidized aluminum (where the Al $2p_{1/2}$ and Al $2p_{3/2}$ contributions are not resolved).[22]

The intensity of the most representative ions specific for nylon-6.6 measured with ToF-SIMS are presented in Figure 2 (the reference polyamide spectra can be found in the Supporting Information). The intensities have been normalized by the total intensity of the spectra for comparison purposes. Their intensity is higher in the weld than outside the weld and the reference and nearly doubles (see Figure 2c). Nonetheless, the intensities of these ions in the reference are already high, meaning that the polymer is already present in the reference. This is in good agreement with the observations made with XPS. There is polyamide-6.6 adsorbed on all the different zones due to the spin-coating process, but in the weld, there is more polyamide adhering on the surface after the dissolution process. In all cases, polyamide-6.6 binds to the


https://doi.org/10.1021/acsomega.1c04264
ACS Omega 2021, 6, 33482−33497

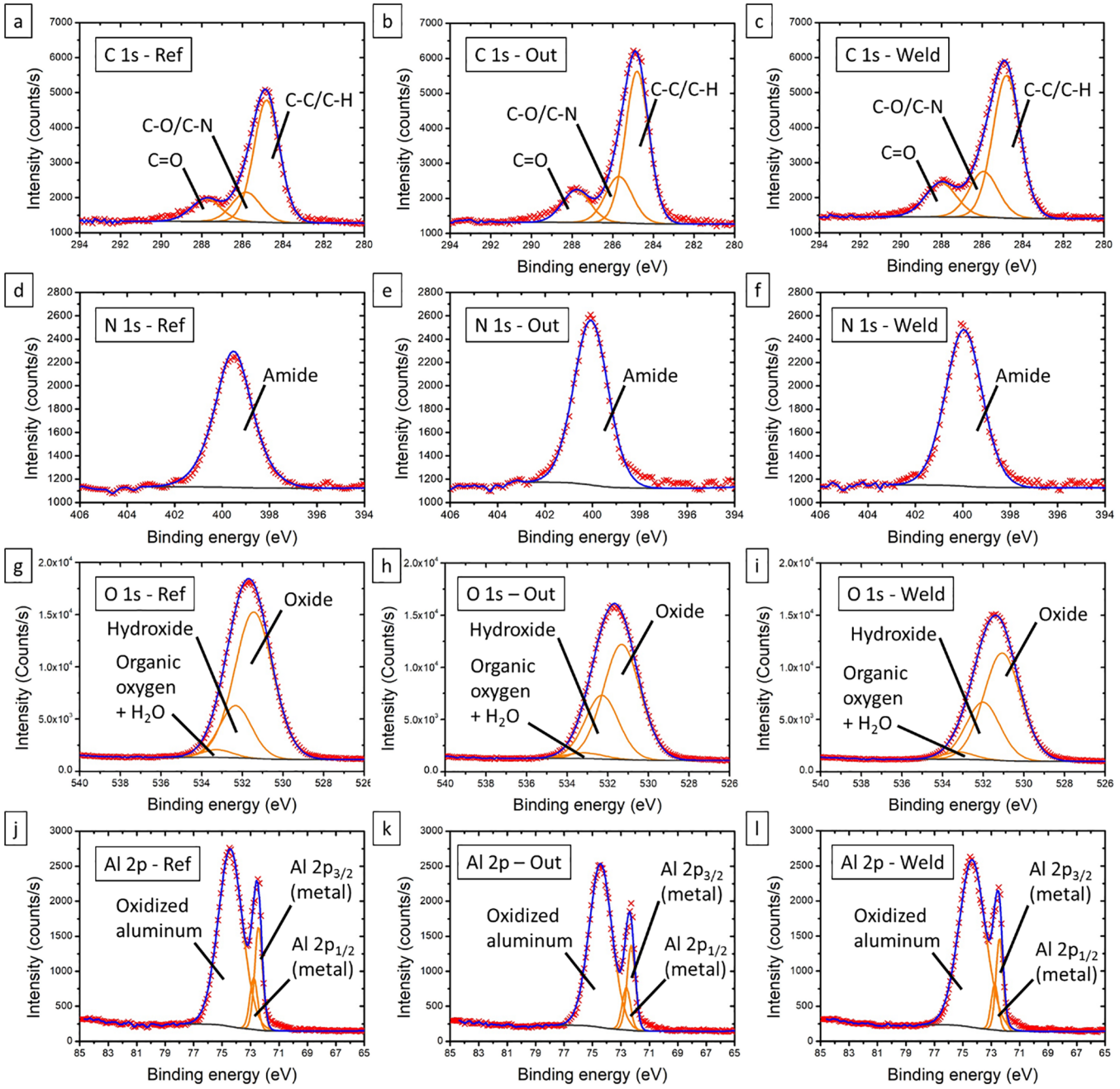


**Figure 1.** XPS high-resolution of the C 1s regions in (a) the reference, (b) out of the weld, and (c) in the weld; of the N 1s regions (d) in the reference, (e) out of weld, and (f) in the weld, of the O 1s regions of (g) the reference, (h) the out of weld, and (i) in the weld; and the Al 2p regions of (j) the reference, (k) out of the weld, and (l) in the weld.

surface, even in "cold" conditions (spin-coating), but more polymers appear to bind in the weld zone ("hot" conditions).

*2.1.2. Chemical Reactivity.* The dissolution step does not remove all the polymers as shown above, but in the weld, higher amounts of the polymer are detected. The polymer melts during the laser welding process as the temperature goes up to 300 °C.[7] This temperature appears to activate a reaction that increases the interactions at the interface, explaining why more polymers are detected in the weld. In the adhesion theory,[27] the only effect that can explain this behavior is chemical bonding. The question is now to determine the bond's nature and the reaction mechanism. Having a look at the polyamide-6.6 chemical formula, depicted in Figure 3, five reactive sites can be identified (marked with red stars). They can be categorized into three types of sites: three carbon reactive sites, a nitrogen reactive site, and an oxygen reactive site. The reactivity of the carbon sites will not be discussed, as the XPS data shows no aluminum carbide peak around 283 eV (see Figure 1a–c). Furthermore, the formation of aluminum carbide seems rather complicated[28−34] and is unstable in the presence of moisture and more generally in the presence of oxygen atoms. As polyamide-6.6 contains moisture,[35] the formation of a carbide bond appears as impossible. In addition, the low probability of aluminum carbide formation was already discussed previously.[17]

*2.1.2.1. Reactivity at the Nitrogen Site.* Looking at the XPS high-resolution spectra from the N 1s region (see Figure 1d–f), only one contribution at 399.8 eV related to the amide


https://doi.org/10.1021/acsomega.1c04264
ACS Omega 2021, 6, 33482−33497

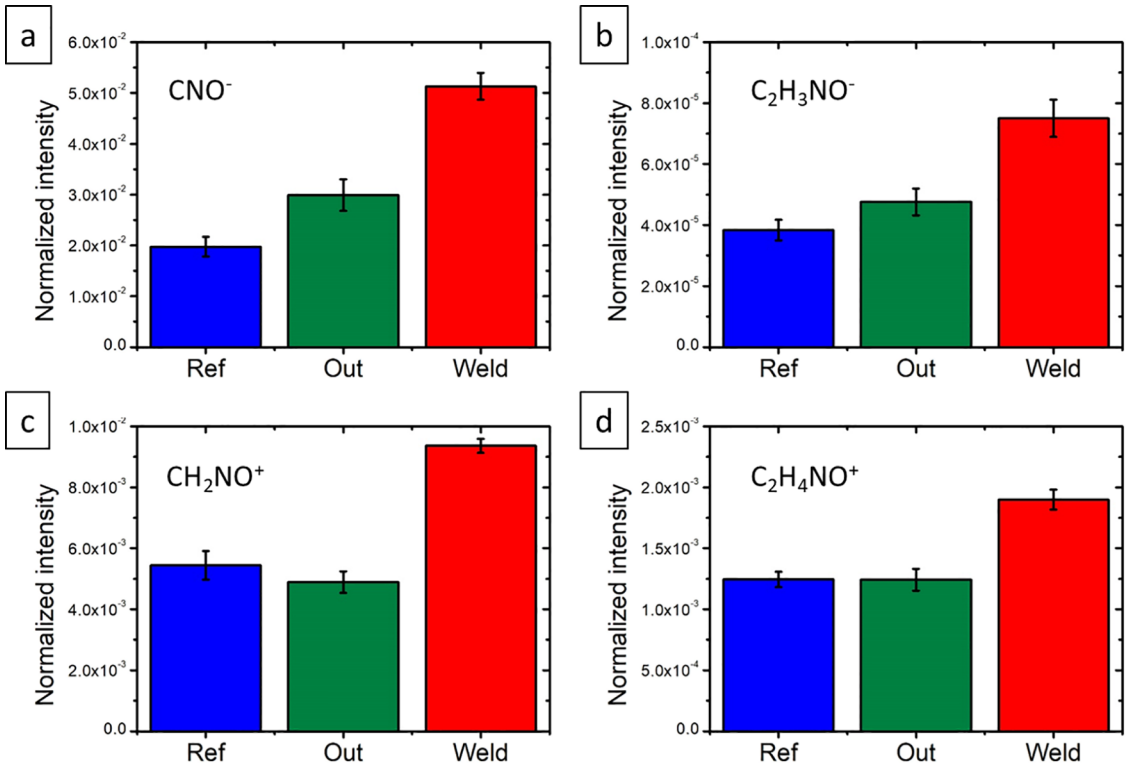


**Figure 2.** ToF-SIMS total counts normalized intensity of characteristic peaks are presented as histograms per zone: in blue, the reference; in green, the out of weld; and in red, the weld of (a) $CNO^-$, (b) $C_2H_3NO^-$, (c) $CH_2NO^+$, and (d) $C_2H_4NO^+$.

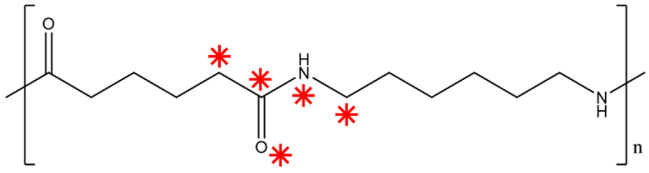

**Figure 3.** Chemical formula of nylon-66 showing the reactive sites by red stars on the chain.

function of the polymer is visible. No contribution from an aluminum nitride bond is identified around the expected 396 eV binding energy.[36−38] If such bonds occurred, their occurrence would be limited and their related intensity would be below the detection limit of the XPS system. In the ToF-SIMS data, only four ions from the family $C_xH_yN_zAl_w^{-/+}$ were surely identified and are presented in Figure 4. Their intensity variations are inconsistent. $CHNAl^{-/+}$ have a higher relative intensity in the weld, nearly twice more, which would be in favor of a C−N−Al bond. However, the following ion $CH_2NAl^-$ has lower relative intensity in the weld compared to the out of weld and the reference, while $CH_2NAl^+$ has equivalent relative intensities for all the three zones. These ions could be preferentially formed by recombination of two neighboring species emitted simultaneously. This recombination hypothesis is supported by the comparison with the $C_xH_yN_zO_wAl_u^{-/+}$ ions intensities (see the next section), which are significantly higher, although these ions are more complex. Figure 5 compares the intensities of $CHNAl^-$, $CHNOAl^-$, $CHNAl^+$, and $CHNOAl^+$, along with $CN^-$ and $CNO^-$, in the weld. The ion $CNO^-$, which could be a source of recombination for the $C_xH_yN_zO_wAl_u^{-/+}$ ions, has a lower intensity than $CN^-$ that is responsible for the recombination of $C_xH_yN_zAl_w^{-/+}$. This tends to prove that the $CHNAl^{+/-}$ ions are formed mainly by recombination but that the $CHNOAl^{+/-}$ ions are formed mainly by direct emission, as will be discussed further. One could argue that the $C_xH_yN_zAl_w^{-/+}$ ions correspond to direct emission from C−N−Al bonds, but these ions would be less stable or present a lower emission probability than the $C_xH_yN_zO_wAl_u^{-/+}$ ions. In that case, to get such intensity, the number of corresponding bonds should be very high, hence detectable in XPS, which is not the case here. Furthermore, the literature is not supporting a C−N−Al bond at the interface because nitrides are peculiarly unstable in the presence of moisture,[39−42] and the present coating and heating experiments were not performed under a controlled atmosphere, i.e., certainly in the presence of moisture. Therefore, the hypothesis of recombination appears as the most probable for the $C_xH_yN_zAl_w^{-/+}$ series of ions. Another source for these ions could also be the direct emission of $C_xH_yN_zO_wAl_u^{-/+}$ ions from the surface followed by oxygen loss, which would support a C−O−Al bond.

*2.1.2.2. Reactivity with the Oxygen Site.* In the XPS high-resolution spectra from the O 1s region, three different contributions were used to fit the spectra (see Figure 1). One at 531.4 eV related to the aluminum oxide, one at 532.3 eV related to the aluminum hydroxide form, and one related to the organic molecule and water at 533.2 eV. The last contribution was related mostly to the amide function and water, but it is reasonable to add a C−O−Al contribution here as well.[17] In the C 1s region, such contribution would be mixed in the C−O/C−N peak around 286 eV. This seems to be a reasonable interpretation, in both spectra, as the C−O−Al bond is similar to C−O−C in terms of electronegativity, henceforth similar in terms of chemical shift in XPS.


https://doi.org/10.1021/acsomega.1c04264
ACS Omega 2021, 6, 33482−33497

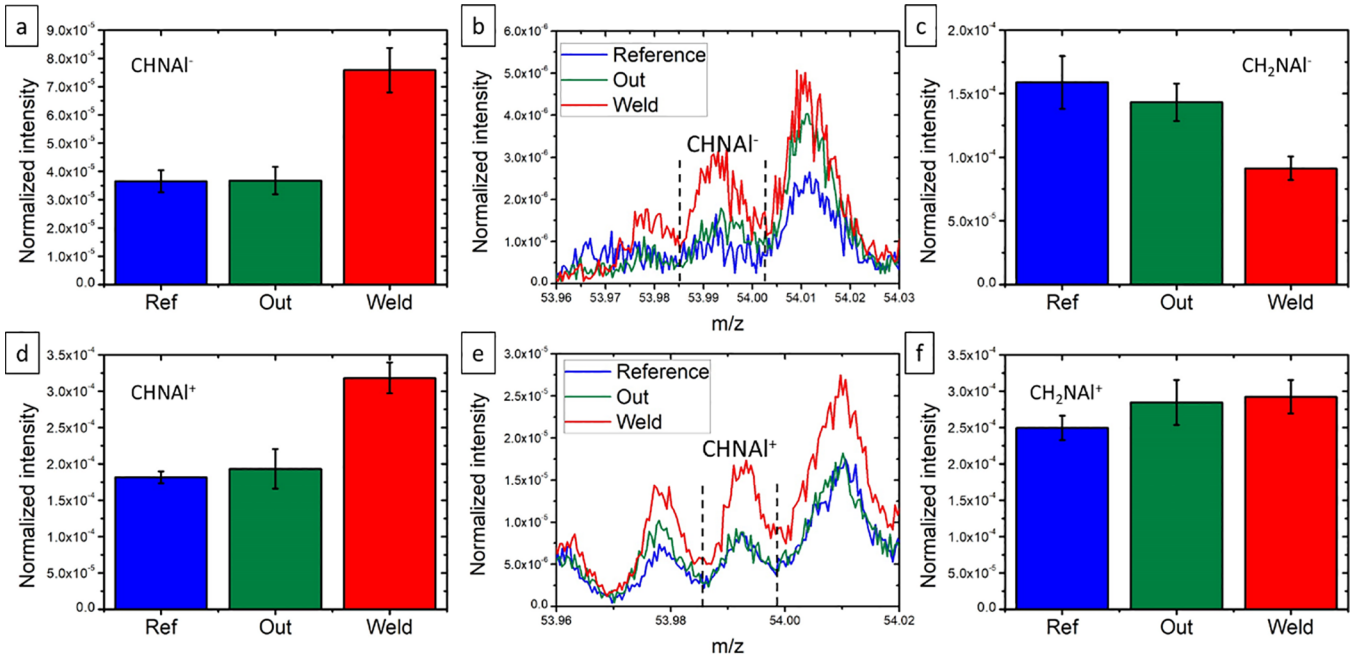


**Figure 4.** ToF-SIMS total counts normalized intensity of characteristic peaks are presented as histograms per zone: in blue, the reference; in green, the out of weld; and in red, the weld of (a) $CHNAl^-$, (c) $CH_2NAl^-$, (d) $CHNAl^+$, and (f) $CH_2NAl^+$, and the mass spectra zone with the range of interest marked by dashed lines of (b) $CHNAl^-$ and (e) $CHNAl^+$.

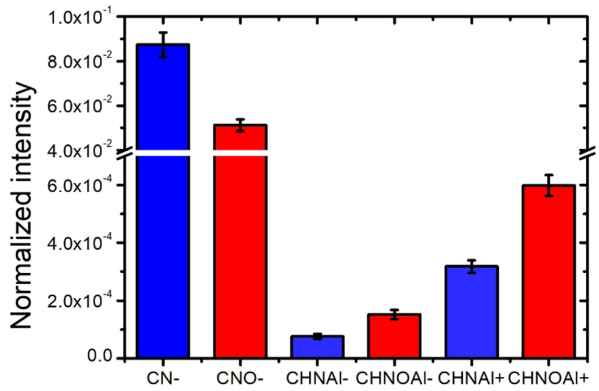


**Figure 5.** Comparison of the normalized intensities of $CN^-$, $CNO^-$, $CHNAl^-$, $CHNOAl^-$, $CHNAl^+$, and $CHNOAl^+$ in the weld.

The SIMS data analysis allowed to identify two families of ions related to a C−O−Al bond: $C_xH_yO_zAl_k^{-/+}$ and $C_xH_yN_zO_wAl_u^{-/+}$.

The ions from the $C_xH_yO_zAl_k^{-/+}$ family (see the Supporting Information) have an erratic behavior; indeed, some of them have equivalent or lower intensities in the weld than outside ($CH_2OAl^-$, $C_2H_2OAl^-$, $C_2H_3OAl^-$, and $C_2H_5OAl^-$ and $CH_4OAl^+$, $C_2H_4OAl^+$, and $C_3H_4OAl^+$), whereas others have higher intensities in the weld ($COAl^-$, $CHOAl^-$, $C_2OAl^-$, $C_2HOAl^-$, and $CO_2Al^-$ and $CHOAl^+$, $CH_3OAl^+$, $C_2HOAl^+$, $C_2H_2OAl^+$, and $CHO_2Al^+$). The first ions, lower in intensity, can be explained by adventitious hydrocarbons and $CO_2$ adsorption on the aluminum surface,[19,21,43] while the second ions, higher in intensity, can be interpreted as originating from the C−O−Al bond or because of a recombination.

Ions from the family $C_xH_yN_zO_wAl_u^{-/+}$ were confidently identified, as $CNOAl^-$, $CHNOAl^-$, $CH_2NOAl^-$, $CHNO_2Al^-$, $CH_2NO_2Al^-$, and $CH_3NO_2Al^-$ and $CNOAl^+$, $CHNOAl^+$, $CHNO_2Al^+$, and $CH_3NO_2Al^+$. They all present higher relative intensities in the weld compared to the out of weld and the reference, as can be seen for some of the ions in Figure 6. These ions could originate from a C−O−Al bond, a C−N−Al bond, or simply a recombination. As discussed above, a C−N−Al bond is not the favored bond (see section 2.1.2.1). Recombination from $CNO^-$, $H^{-/+}$, and $Al^{-/+}$ to form these ions is possible and some of the ions detected might originate from it. Nonetheless, as was noticed in Figure 5, the intensity of $CNO^-$ is much lower than the intensity of $CN^-$, but at the same time, the ions $CHNOAl^{-/+}$ have higher intensities than the $CHNAl^{-/+}$ ions. If only recombination occurred, the ions $CHNOAl^{-/+}$ would have lower intensities than $CHNAl^{-/+}$ ions. This is even truer since the heavier the ion is, the lower the probability is to produce it by recombination. Therefore, the more probable explanation is that there is a C−O−Al bond that formed during the welding. Literature studies show several examples of such bonds between polyimides and aluminum.[44−48] The polymer already binds to the surface during the spin-coating process, but the welding process allows the polymer to melt and to rearrange itself by reptation[7,49] again, enabling the polymer to expose the C═O reactive sites toward the aluminum and to create even more bonds between both materials. This allows to clearly identify the bond as a C−O−Al bond as depicted in Figure 7, which is in good agreement with the article of Hirchenhahn *et al.*[17]

*2.1.2.3. Reactivity of the Metal.* Figure 8 depicts the normalized relative intensity of characteristic ions of aluminum oxide and aluminum hydroxide. The relative intensities of the ions related to the oxide are equivalent for all three zones, while the relative intensities of the ions related to the hydroxide are slightly lower in the weld than in the reference. The out of weld has an intermediate behavior for the hydroxide ions. This supports the assumption that the polymer reacts with the free-hydroxyl groups present at the surface during the welding process.


https://doi.org/10.1021/acsomega.1c04264
ACS Omega 2021, 6, 33482−33497

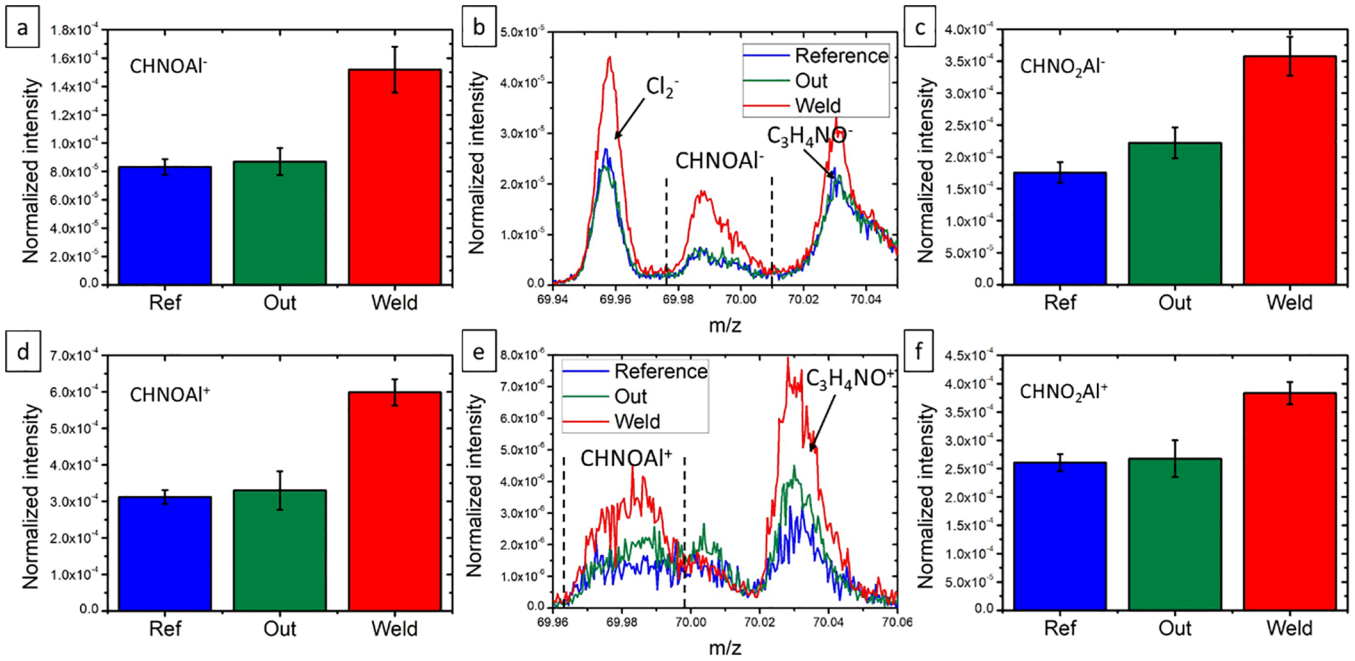


**Figure 6.** ToF-SIMS total counts normalized intensity of characteristic peaks are presented as histograms per zone: in blue, the reference; in green, the out of weld; and in red, the weld of (a) $CHNOAl^-$, (c) $CHNO_2Al^-$, (d) $CHNOAl^+$, and (f) $CHNO_2Al^+$ and the mass spectra zone with the range of interest marked by dashed lines of (b) $CHNOAl^-$ and (e) $CHONAl^+$.

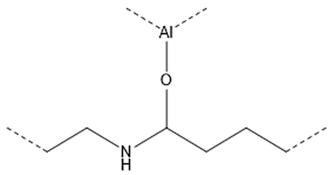


**Figure 7.** Scheme of the chemical bond between the aluminum surface and polyamide-6.6.

Figure 9a shows the percentage of aluminum obtained from the XPS survey for the three zones. The percentage is equivalent in all zones, especially the reference and the weld. The oxidized layer thickness was calculated using Strohmeier's method[50] from the high-resolution spectra in the Al 2p region (see Figure 9b). It is noticeable that the oxidized layer is thicker in the weld than in the reference, the out of weld being in an intermediate position, even if it mostly looks like the reference. The welding seems to oxidize the metal surface deeper. This might partly be due to the fact that the reaction of the polymer with the metal releases water, as depicted in Figure 10. Moreover, water is also present in the polymer naturally, which also might be the source of oxygen atoms to oxidize the aluminum surface.[35] To sum up, the laser welding heats up the metal, activating the oxidation reaction in the weld, which leads to a thicker native oxide layer at this place. This oxidation can only take place with a source of oxygen, which is the case with the polymer itself by reacting as proposed in Figure 10, or with the moisture present.[35]

**2.2. Model Samples.** *2.2.1. Surface Composition.* Table 2 summarizes the average elemental composition obtained by analyzing the XPS survey spectra for the UV-cleaned samples, the air-dried samples, and the heated samples. The nitrogen percentage is three times higher on the heated samples than the UV-cleaned samples, while the air-dried samples show intermediate values of nitrogen percentage. A first observation is that the molecule is deposited on the surface of the air-dried and heated samples. A second observation is that the heating has an effect on the molecule's deposition, since there is more nitrogen on the heated samples than on the air-dried samples. This indicates that the molecule is more strongly bound after heating than without heating. On the air-dried samples, some of the methylformamide that deposited have been desorbed. Nonetheless, the percentage of nitrogen is far off from the theoretical value of pure *N*-methylformamide, leading to the conclusion that the film deposited is extremely thin. This is confirmed by looking at the percentages of the other elements. The carbon percentage is quite high on the UV-cleaned samples. This is due to experimental reasons. Indeed, the UV-cleaned samples were transported in air from the cleaner to the XPS machine. It took only a few minutes, but it was sufficient for recontamination. The carbon percentage is relatively low for the air-dried and the heated samples. Maybe the very thin layer of methylformamide deposited on the substrate prevents the recontamination of the surface after dipping. At the same time, the oxygen percentage is higher in the air-dried and heated samples, which would also support the idea that the methylformamide limits the recontamination by blocking the reactive sites. The aluminum percentage is equivalent on the UV-cleaned and the heated samples but is slightly higher on the air-dried samples.

The XPS high-resolution spectra of the C 1s region depicted in Figure 11a–c, were fitted using four contributions. The first one is attributed to C–C/C–H bonds at 284.8 eV and was used for calibration. The second contribution at 286.1 eV is attributed to C–O and C–N bonds. The third one at 288.2 eV is attributed to a C═O function. The fourth one at 289.5 eV is attributed to carbonate.[22] This shows that the surfaces are contaminated with adventitious hydrocarbons and carbonate; for the air-dried and the heated samples, the presence of well-defined C–O/C–N and C═O peaks shows that methylformamide was deposited on the surface.


https://doi.org/10.1021/acsomega.1c04264
ACS Omega 2021, 6, 33482–33497

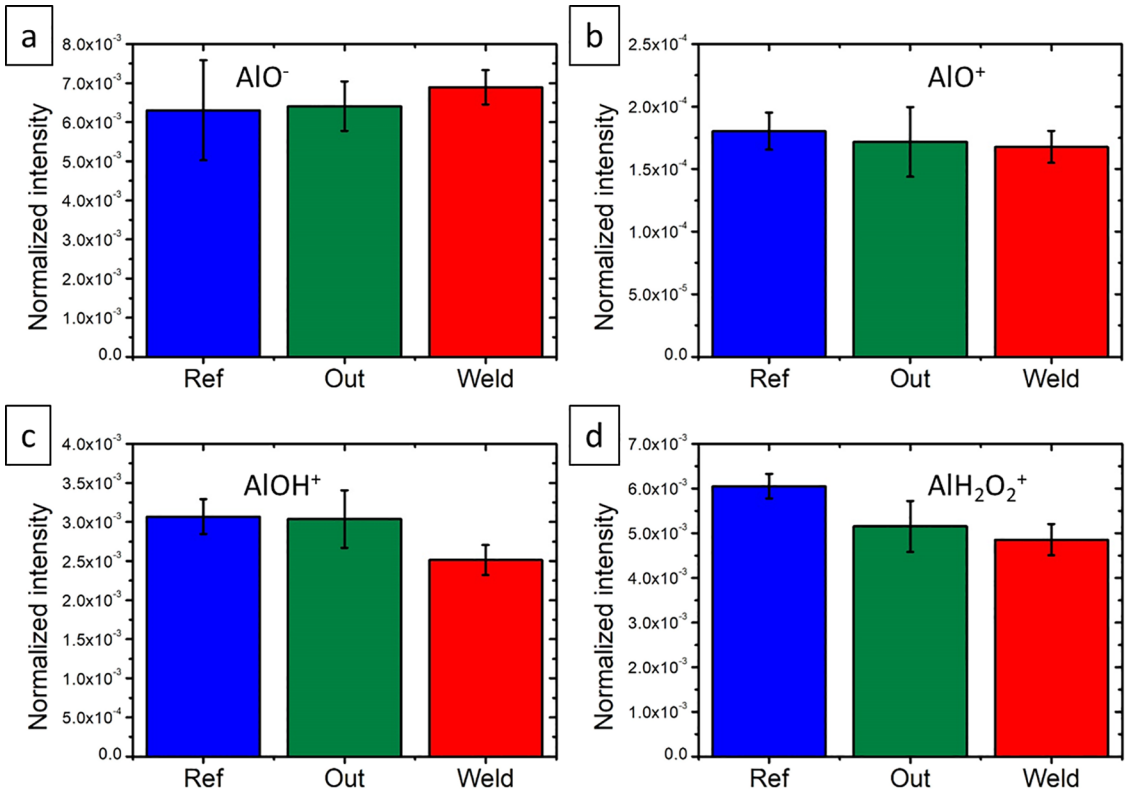


**Figure 8.** ToF-SIMS total count relative intensity of characteristic ions of an oxidized aluminum surface: (a) $AlO^-$, (b) $AlO^+$, (c) $AlOH^+$, and (d) $AlH_2O_2^+$.

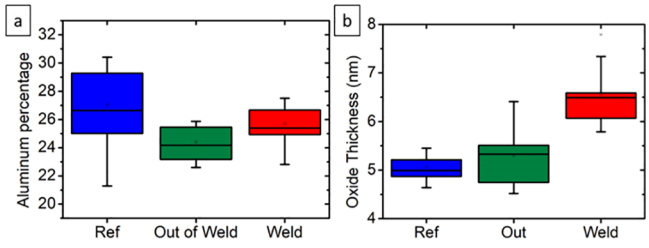


**Figure 9.** (a) Percentage of aluminum obtained from the XPS survey spectra per zone; (b) oxide thickness per zone calculated from the XPS Al 2p region using Strohmeier's method.[50]

**Table 2. XPS Average Elemental Composition and its Standard Deviation of UV-Cleaned Aluminum, the Air-Dried samples, and Heated Samples and the Theoretical Composition of *N*-Methylformamide**

| samples | % Al | % O | % C | % N |
|---|---|---|---|---|
| UV-cleaned | 28.3 (±1.2) | 44.7 (±0.9) | 26.3 (±1.7) | 0.6 (±0.2) |
| air-dried | 32.0 (±1.7) | 53.1 (±1.5) | 14.0 (±3.1) | 1.0 (±0.2) |
| heated | 29.0 (±2.4) | 53.9 (±3.4) | 15.3 (±5.0) | 1.8 (±0.2) |
| *N*-methylformamide | | 25 | 50 | 25 |

The O 1s regions, which spectra are presented in Figure 11d–f, were fitted using three contributions. The first one at 531.4 eV is interpreted as aluminum oxide, the second one at 532.4 eV is related to aluminum hydroxide, and the last one at 533.5 eV is due to organic molecules and water. This interpretation is relatively classical for an aluminum surface exposed to air.[22,25,26] The last contribution is slightly more intense for the air-dried samples and even more intense on the heated samples, which indicates a chemical difference in the

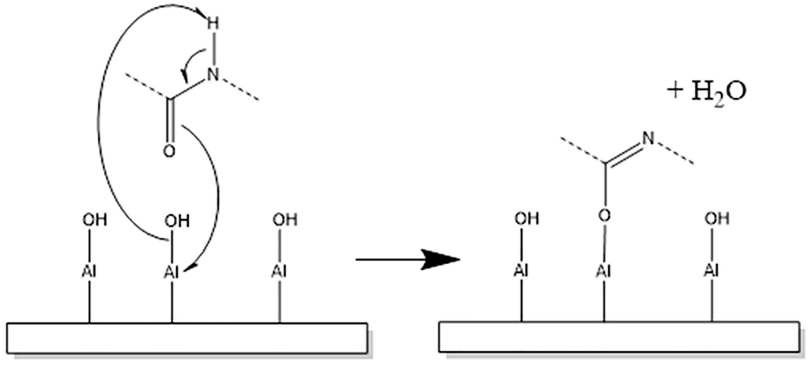


**Figure 10.** Scheme of the reaction mechanism between the polyamide-6.6 and the aluminum surface.



https://doi.org/10.1021/acsomega.1c04264
ACS Omega 2021, 6, 33482−33497

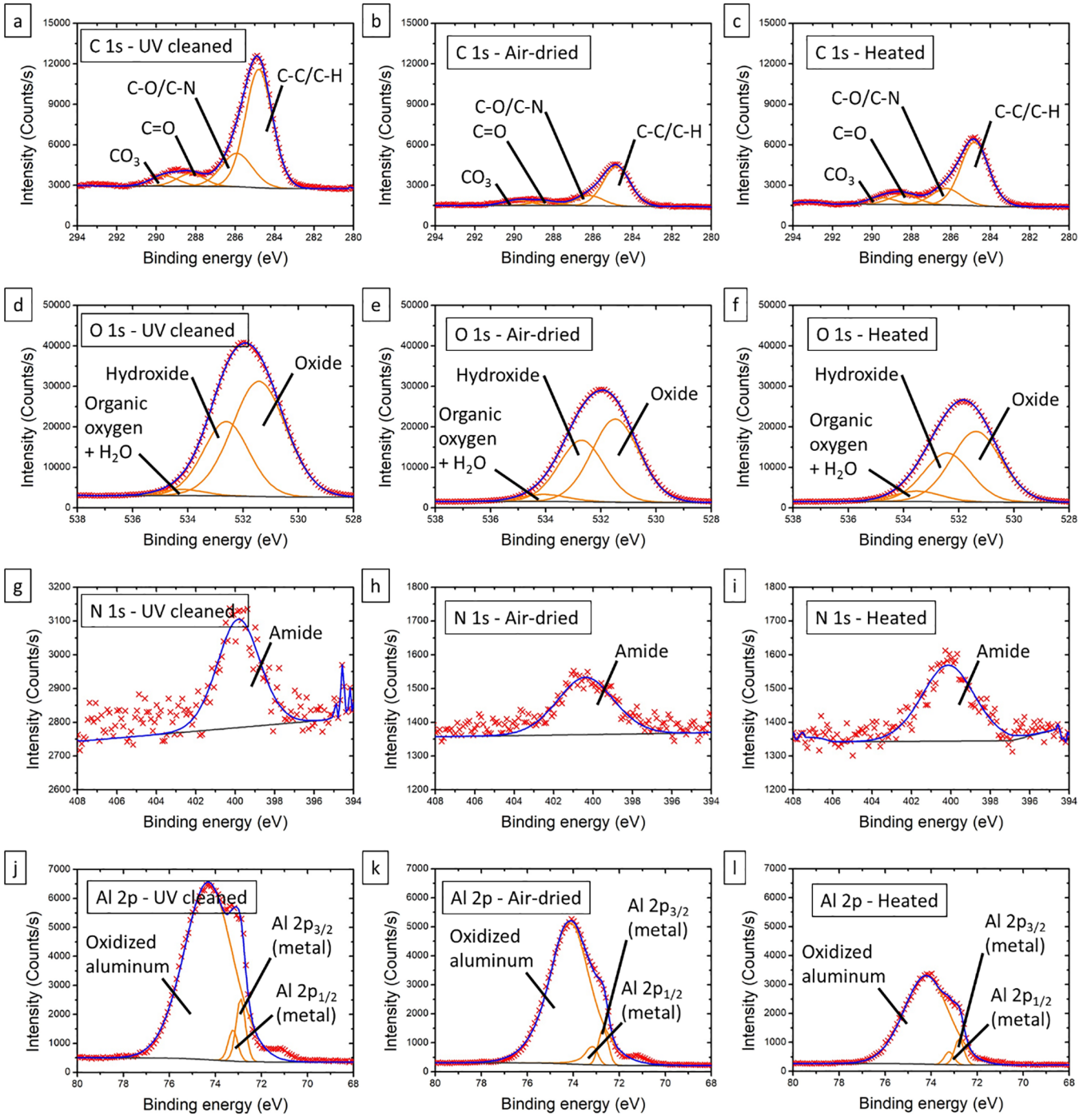


**Figure 11.** XPS high-resolution spectra of the C 1s region for (a) the UV-cleaned samples, (b) the air-dried samples, and (c) the heated samples, of the O 1s region for (d) the UV cleaned samples, (e) the air-dried samples, and (f) the heated samples, of the N 1s region for (g) the UV cleaned samples, (h) the air-dried samples, and (i) the heated samples, and of the Al 2p region for (j) the UV cleaned samples, (k) the air-dried samples, and (l) the heated samples.

organic oxygen on the top surface. This supports the assumption that methylformamide molecules are deposited on the surface.

The XPS high-resolution spectra of the N 1s region, shown in Figure 11g–i, are of low intensity since there is only about 1–2% nitrogen detected in the survey spectra. Even if the noise-to-signal ratio is very high, only one contribution at 399.9 eV is observed on the air-dried and heated samples, which is a characteristic peak for amides.[22] This confirms that some methylformamide is present on the surface after the dip-coating and the two different drying processes. The nitrogen signal compared to the noise amplitude is too low on the UV-cleaned samples to draw any conclusion.

For the XPS high-resolution spectra of the Al 2p region, presented in Figure 11j–l, three contributions were used for fitting. The first two at 72.8 and 73.2 eV are attributed to Al $2p_{3/2}$ and Al $2p_{1/2}$ and are both due to aluminum in its metallic form. The last contribution at 74.2 eV is attributed to oxidized aluminum.[22] This is the typical spectra of an aluminum surface covered by its native oxide.[51−60]



https://doi.org/10.1021/acsomega.1c04264
ACS Omega 2021, 6, 33482−33497

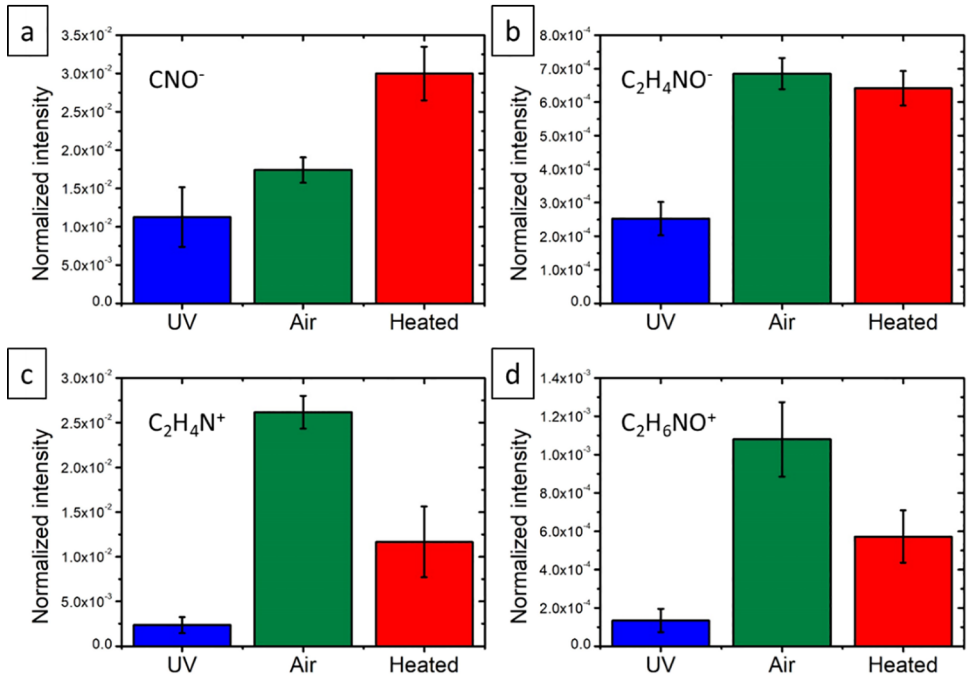


**Figure 12.** ToF-SIMS total counts normalized intensity of characteristic peaks of methylformamide presented as histograms per samples: in blue, the UV-cleaned samples; in green, the air-dried samples; and in red, the heated samples of (a) $CNO^-$, (b) $C_2H_4NO^-$, (c) $CH_4N^+$, and (d) $C_2H_6NO^+$.

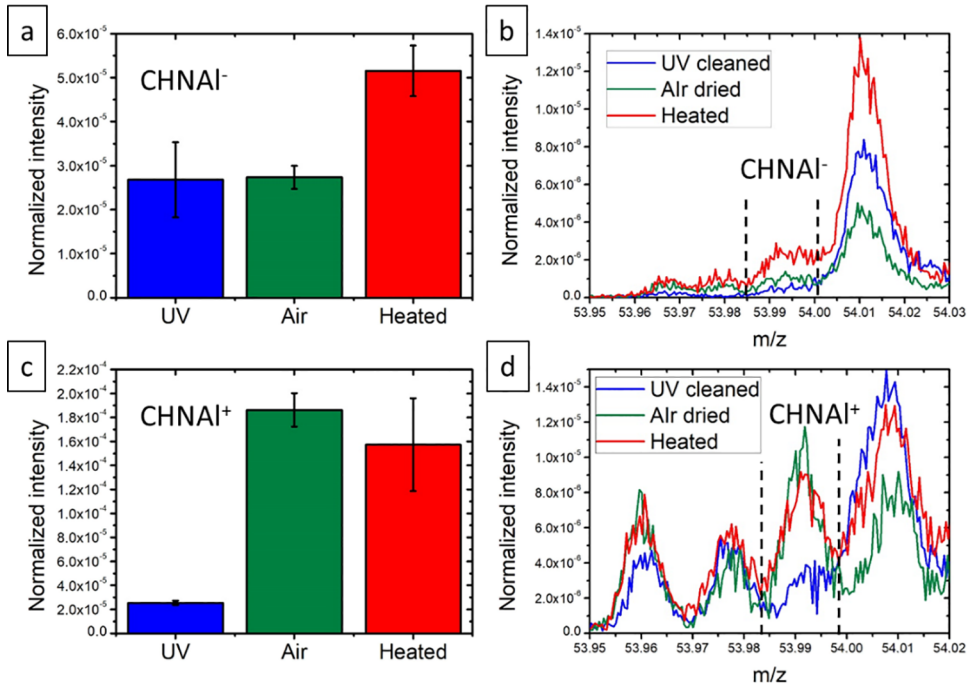


**Figure 13.** ToF-SIMS total counts normalized intensity of characteristic peaks presented as histograms per zone: in blue, the UV-cleaned samples; in green, the air dried ones; and in red, the heated samples and the mass spectra with the range of interest marked by dashed lines of (a, b) $CHNAl^-$ and (c, d) $CHNAl^+$.

In Figure 12, the relative ToF-SIMS intensities (normalized to the total intensity of the spectra) of characteristic ions for *N*-methylformamide are presented: $CNO^-$, $C_2H_4NO^-$ ($[M - H]^-$), $CH_4N^+$, and $C_2H_6NO^+$ ($[M + H]^+$). They all present higher relative intensities for the air-dried and heated samples. This confirms clearly the deposition of methylformamide after the dip coating. However, by comparing the relative intensities of these ions of the air-dried and heated samples, the $[M + H]^+$ and $CH_4N^+$ ions have much lower intensities after heating. This seems to contradict the XPS data, where more nitrogen is detected on the heated samples. On the other hand, the relative intensity of the $CNO^-$ fragment is much higher on the heated samples, while the intensity of $C_2H_4NO^-$ is equivalent for both samples. This is also true for $C_2H_4NO^+$ (see the


https://doi.org/10.1021/acsomega.1c04264
ACS Omega 2021, 6, 33482−33497

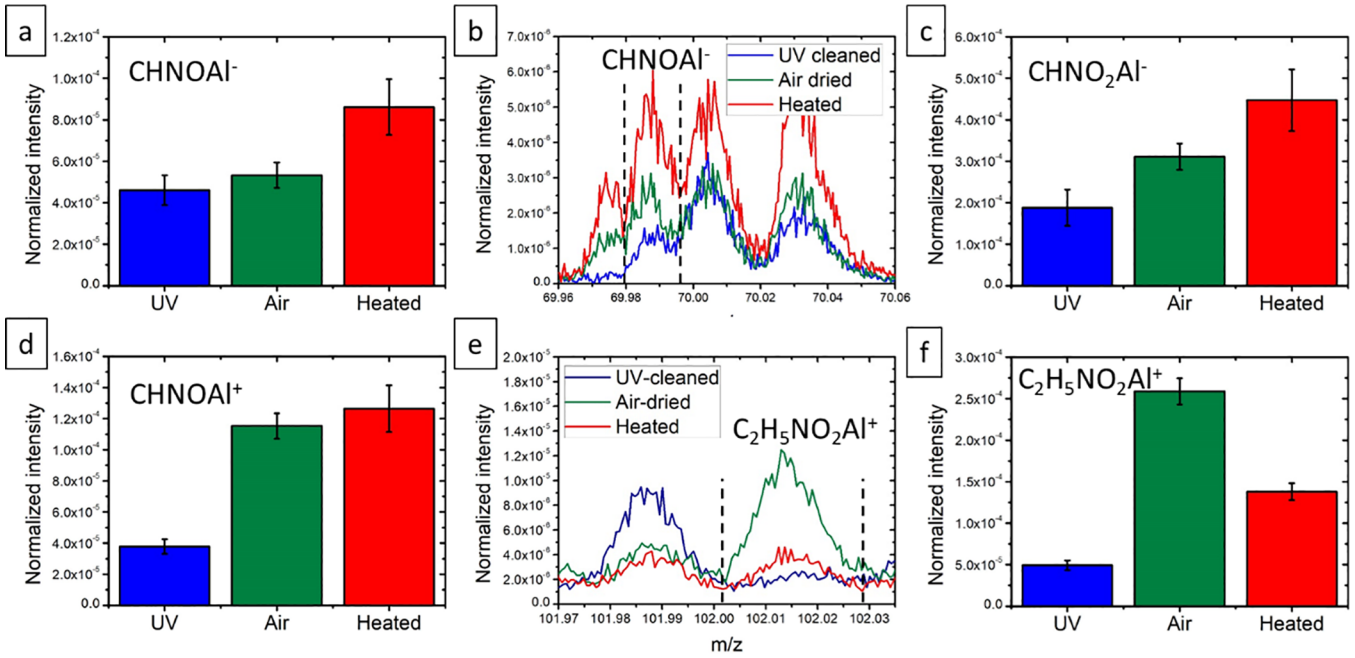


**Figure 14.** ToF-SIMS total counts normalized intensity of characteristic peaks presented as histograms per zone: in blue, the UV cleaned samples; in green, the air-dried ones; and in red, the heated samples of (a) $CHNOAl^-$, (c) $CHNO_2Al^-$, (d) $CHNOAl^+$, and (f) $C_2H_5NO_2Al^+$, and the mass spectra zone with the range of interest marked by dashed lines of (b) $CHNOAl^-$ and (e) $C_2H_5NO_2Al^+$.

Supporting Information). The hydrogen-rich ions have lower intensities after heating, while the hydrogen-poor ions are more or equivalently intense. This points to the direction of a reaction at the interface between the *N*-methylformamide and the aluminum. Since there is more nitrogen detected after heating, one can conclude that there is a bonding reaction between both components. As the hydrogen-rich ions are less intense after the heating, this suggests that hydrogen is lost by the *N*-methylformamide during the reaction. This will be investigated hereafter.

*2.2.2. Chemical Reactivity.* As said above, these samples were designed to elucidate the reaction mechanism between an amide function and an aluminum surface. The molecule selected, *N*-methylformamide, is composed of only the amide function, presenting the same reactive sites as on polyamide-6.6: carbon reactive sites, a nitrogen reactive site, and an oxygen reactive site. The reactivity of the carbon reactive sites will not be discussed for the same reasons as for the spin-coated samples: no carbide peak on the XPS high-resolution C 1s spectra and low probability of carbide formation in the presence of moisture and oxygen reactive sites.

*2.2.2.1. Reaction of the Nitrogen Sites.* From the XPS high-resolution spectra of the N 1s region (see Figure 11g–i), it appears that there is no Al–N peak around 396 eV.[36−38] However the signal of the nitrogen is very low because there is only 1–2% on the surface, so the interpretation of the spectra is rather uncertain. Nonetheless, it is consistent with the previous experiments on the welded samples and the spin-coated samples.

In ToF-SIMS, only two ions of the $C_xH_yN_zAl_w^{+/-}$ series were identified: $CHNAl^+$ and $CHNAl^-$ (see Figure 13). $CHNAl^-$ is twice more intense on the heated samples compared to the UV-cleaned and air-dried samples. However, this ion has a very low relative intensity of $\sim 5.10^{-5}$, which tends to indicate a recombination. This ion is actually barely noticeable on the spectrum. For comparison, the $CHNOAl^-$ ion has an intensity of $\sim 5.10^{-4}$, therefore 10 times more intense. $CHNAl^+$, on the contrary, presents higher intensities on the air-dried and the heated samples, which is consistent to the fact that there is less nitrogen present in the UV-cleaned samples (see Table 2). The intensity on the air-dried and the heated samples is equivalent despite the fact that there is more nitrogen and despite the effect of heating on the heated samples. This is in favor of recombination. As discussed above (see section 2.1.2.1), the formation of these ions could also originate just from a C–N–Al bond and present a lower emission probability or stability. Similarly, if that were the case, a huge number of bonds would be present, therefore detectable in XPS, which is also not the case on these samples. Therefore, the hypothesis of recombination is favored.

*2.2.2.2. Reaction of the Oxygen Sites.* As described above, the XPS high-resolution spectrum of the O 1s region was fitted using three contributions (see Figure 11). Two are associated to the aluminum oxide and hydroxide, respectively. The third one at 531.4 eV was assigned to organic components and water. As described in sections 2.1.1, 2.1.2.2, and 2.2.1, this peak could also be attributed to C–O–Al. This is supported by the spectra of the C 1s region, with the peak at 286.1 eV, which could also correspond to such type of bond.

The SIMS data analysis allowed identific ation of two families of ions related to a C–O–Al bond on these samples as well: $C_xH_yO_zAl_k^{+/-}$ and $C_xH_yN_zO_wAl_u^{+/-}$.

As on the other samples, the $C_xH_yO_zAl_k^{+/-}$ ions (see S.I.) have an erratic behavior. Some of them have equivalent intensities on all samples, or lower intensities on the heated samples compared to the UV-cleaned or air-dried samples ($CH_2OAl^+$, $CH_3OAl^+$, $CH_4OAl^+$, and $C_2OAl^-$, $C_2HOAl^-$, $CO_2Al^-$). While a few of these ions have higher intensities on the heated samples compared to the UV cleaned and air-dried samples ($CHOAl^+$ and $COAl^-$, $CHOAl^-$). In the negative mode, the ions with the lowest intensities on the heated samples have a composition that could be related to


https://doi.org/10.1021/acsomega.1c04264
ACS Omega 2021, 6, 33482–33497

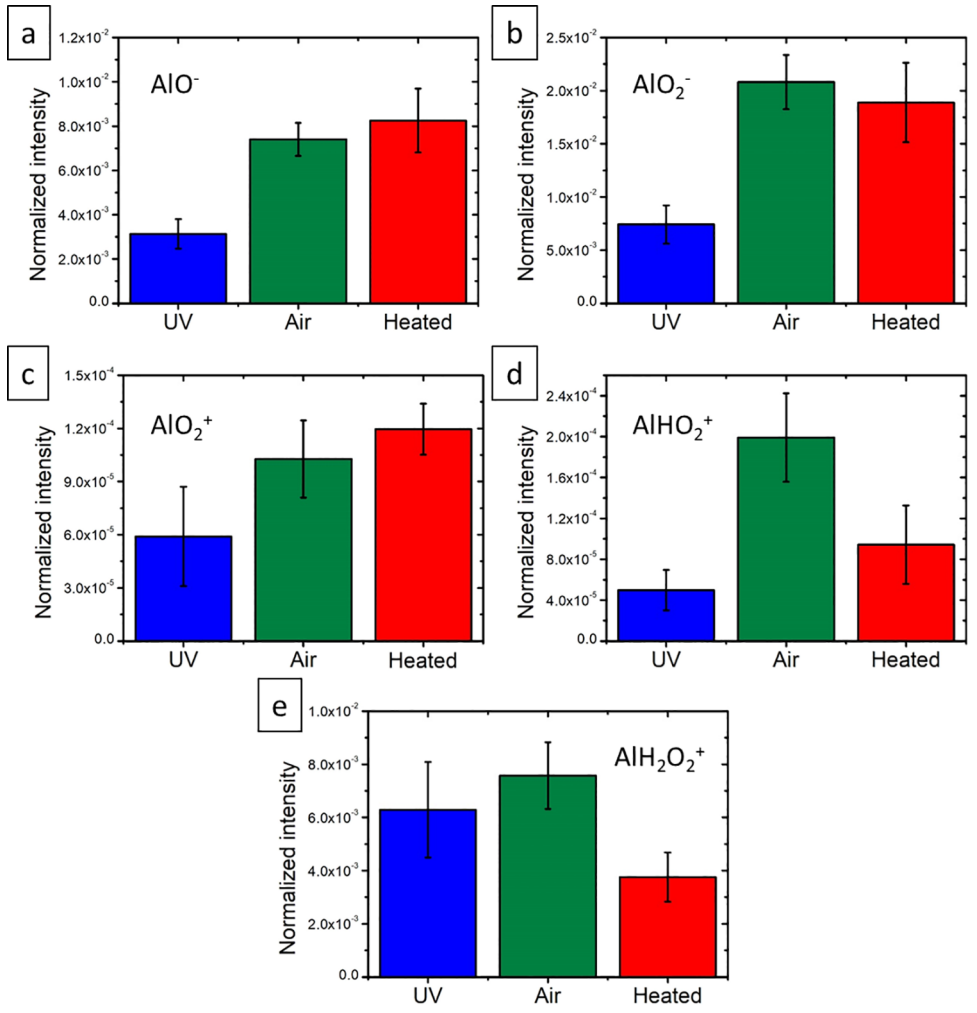


**Figure 15.** ToF-SIMS total count relative intensity of characteristic ions of an oxidized aluminum surface: (a) $AlO^-$, (b) $AlO_2^-$, (c) $AlO_2^+$, (d) $AlHO_2^+$, and (e) $AlH_2O_2^+$.

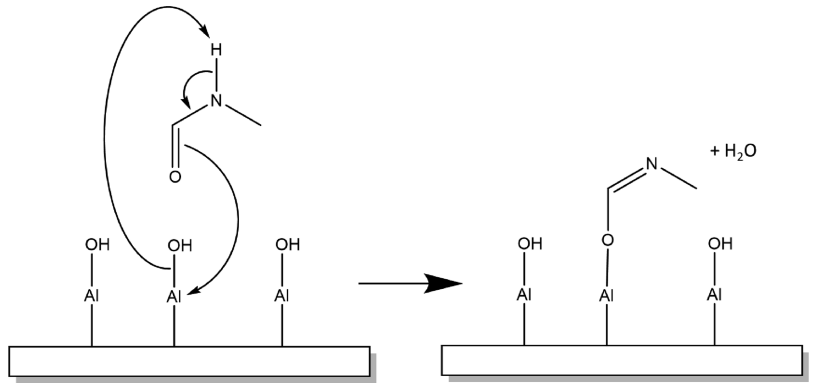


**Figure 16.** Proposition of the reaction mechanism between the molecule and the metal surface.

adventitious hydrocarbons and carbon dioxide contamination on an aluminum surface. These ions are therefore not good indicators of the interface bonds.

The $C_xH_yN_zO_wAl_u^{+/-}$ family of ions are the negative mode; only three ions of this family could be surely identified: $CNOAl^-$, $CHNOAl^-$, and $CHNO_2Al^-$. In the positive mode, these ions are more diverse than the other samples: $CHNOAl^+$, $CH_3NOAl^+$, $CHNO_2Al^+$, $C_2H_5NOAl^+$, $C_2H_6NOAl^+$, $CH_3NO_2Al^+$, and $C_2H_5NO_2Al^+$. Some of the ions' intensities are presented in Figure 14. On the air-dried samples, most of the ions' intensities are lower than on the heated samples, which points in the direction of a C−O−Al bond formation. However, as for $C_2H_5NO_2Al^+$, the intensity is much higher on the air-dried samples than on the heated samples. This ion is composed of the entire methylformamide molecule and an AlO fragment of the metal surface. In section 2.2.1, the hypothesis of a binding reaction of the molecule with the surface was proposed. This binding induces changes in the



https://doi.org/10.1021/acsomega.1c04264
ACS Omega 2021, 6, 33482−33497

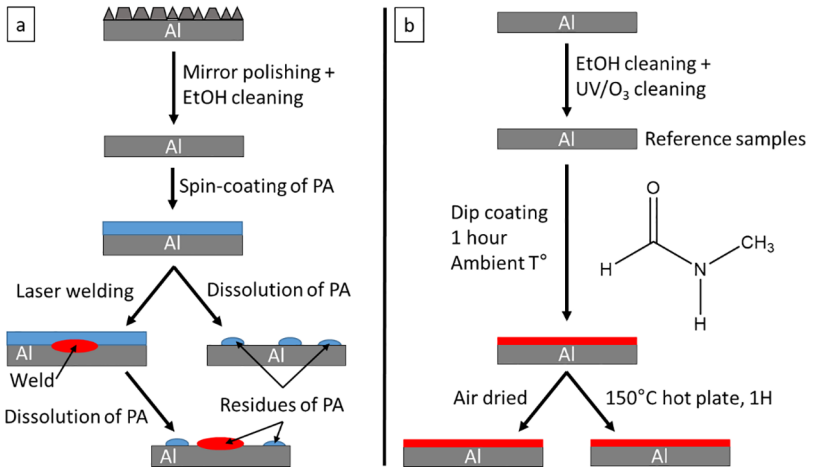


**Figure 17.** Sample preparation (a) for the spin-coated samples and (b) for the dip-coated samples.

molecule, explaining why the ions presenting the whole molecule are less intense on the heated samples. With the nature of these hybrid ions and the results presented above, a C−O−Al bond due to the deposition and heating is the most suitable option.

*2.2.2.3. Reactivity of the Metal.* The percentage of aluminum in the XPS survey spectra on the UV-cleaned and the heated samples is similar, while it is higher on the air-dried samples. The XPS high-resolution spectra of the Al 2p region were fitted using three contributions: two interpreted as from metallic aluminum and one for the oxidized form of aluminum (see section 2.2.1). From this, an estimate of the oxide thickness could be calculated using Strohmeier's method.[50] For the three samples, there was no statistically significant difference, and an average value of nearly 8 nm for the oxide thickness was obtained for all samples (data not provided). Indeed, the heating here is lower than during the welding process, only 150 °C compared to nearly 300 °C, and the methylformamide forms a much thinner deposit than the spin-coated polymer, which diminishes the impact of the chemical reaction at the interface.

Some of the ions detected with ToF-SIMS can give us a clue about the reaction mechanism between polyamide-6.6 and the aluminum surface. The relative intensities of some metallic ions are presented in Figure 15. It can be observed that the hydroxide ions have significantly lower intensities on the heated samples compared to the air-dried samples, see Figure 15d,e. This points to a disappearance of hydroxide during the heating process, following their reaction with methylformamide. At the same time, the intensities of the oxide ions are similar on the air-dried and the heated samples.

As mentioned above in sections 2.2.1 and 2.2.2.2, an observation was made that the molecule on the heated samples tends to lose hydrogen. This was confirmed with the lower intensity of $CH_4N^+$ and $C_2H_6NO^+$, and the lower intensity of $C_2H_5NO_2Al^+$. In Figure 16, a possible reaction mechanism is depicted. The fragmentations of the formed compound during ToF-SIMS measurement are in good agreement with the spectra. Indeed, it explains that the lower intensity of $C_2H_6NO^+$ is because of the loss of a hydrogen atom during the reaction. The lower intensity of $CH_4N^+$ can be explained also by the loss of a hydrogen atom bound to nitrogen but also because presumably, this nitrogen atom has a double bond with carbon after the reaction with the surface (Figure 18),

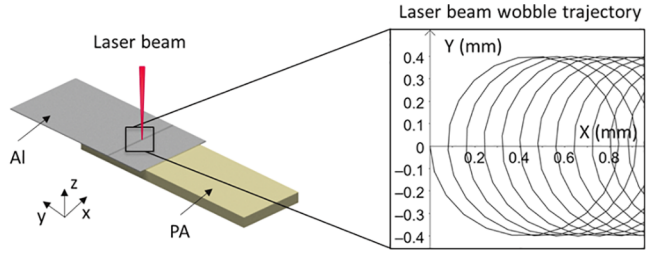


**Figure 18.** Schematic drawing of the laser welding process.

which diminishes the probability of a fragmentation there. The lower intensity on the heated samples for $C_2H_5NO_2Al^+$ is due to the loss of the hydrogen atom bound to nitrogen. The intensities of $CNO^-$ and $C_2H_4NO^-$ are barely affected by this chemical reaction, while the intensities of $CHNOAl^{-/+}$ are also explained by the C−O−Al bond formation.

## 3. CONCLUSIONS

In this work, two different types of samples were analyzed in order to investigate the following: (1) the nature of the chemical bond between polyamide-6.6 and native oxide from an aluminum sheet and (2) the corresponding reaction mechanism. The first types of samples studied were obtained by spin-coating polyamide-6.6 onto mirror polished aluminum, which were then laser welded. The polyamide layer was dissolved to access the interface. XPS and ToF-SIMS measurements were performed in the weld region, out of the weld, and on non-welded samples that served as reference. The second types of samples studied were prepared by dip-coating a layer of *N*-methylformamide, a molecule composed of the reactive part of the polymer, on aluminum plates. Some of the coated aluminum plates were dried at room temperature; the others were heated to simulate laser welding. $UV/O_3$-cleaned aluminum plates served here as references. Three different samples were analyzed by XPS and ToF-SIMS: the reference, the air-dried samples, and the heated samples.

On the spin-coated samples, XPS results detect more nitrogen in the weld zone of the spin-coated samples than elsewhere, and the characteristic peaks of polyamide-6.6 are detected on the high-resolution spectra in all three zones. This shows that polyamide-6.6 is still present after the dissolution step on all the analyzed zones but in larger amounts in the weld. These observations are well supported by the ToF-SIMS


https://doi.org/10.1021/acsomega.1c04264
ACS Omega 2021, 6, 33482−33497

data, as the characteristic ions present higher intensities in the weld. This emphasizes the role of the heating due to the welding on the adhesion between both materials. The possible chemical reactions were investigated first on the polymer as well as on the metal. A reaction with the carbon reactive sites was directly excluded. In XPS, the high-resolution spectra do not present signs of a nitride bond, but its presence might be below the detection limit of the XPS machine. In XPS, the formation of a C−O−Al bond could not be confirmed nor informed. The analysis of the hybrid ions detected in the ToF-SIMS spectra shows that the detected $C_xH_yN_zAl_w^{+/-}$ certainly originates from recombination (probably $CN^-$, $H^{+/-}$, and $Al^{+/-}$), and that the intensity of the ions of the $C_xH_yN_zO_wAl_u^{+/-}$ family can be explained by a C−O−Al bond formation due to the welding. Having a closer look at the high-resolution spectra in the Al 2p region, it was shown that the oxidized layer is slightly thicker in the weld. The weld induces oxidation of the metal at the interface. At the same time in ToF-SIMS, the intensity of the hydroxide ions is lower in the weld than elsewhere, while the intensity of the oxide ions is equivalent. This leads to the conclusion that the reaction between the polymer and the metal happens at the free-hydroxyl groups of the aluminum surface. Based on this, a reaction mechanism was proposed (see Figure 10), where the oxygen of the amide group of the polymer reacts with the free-hydroxyl group of the metal by forming a C−O−Al bond and an imine bond (C═N) while releasing water.

The dip-coating process deposits a very thin *N*-methylformamide layer on aluminum for the air-dried samples as well as for the heated samples. This deposition is confirmed in both XPS and ToF-SIMS, by a higher percentage of nitrogen in XPS and the detection of characteristic ions for an amide molecule on ToF-SIMS. On the heated samples, more *N*-methylformamide is detected than on the air-dried samples because of a higher percentage of nitrogen in XPS, but also, the characteristic ion of *N*-methylformamide presents higher intensities in ToF-SIMS. *N*-Methylformamide reacts with the surface to create more bonds because of the heating. The thickness of the layer is very thin, making the interpretation of the XPS high-resolution spectra difficult as the intensity of the *N*-methylformamide's signal is low. Nonetheless, the ToF-SIMS analysis of the hybrid ions' intensities and especially the $C_xH_yN_zAl_w^{+/-}$, $C_xH_yO_zAl_k^{+/-}$, and $C_xH_yN_zO_wAl_u^{+/-}$ ions allows here to conclude that the bond formed at the interface is certainly a C−O−Al bond, as on the spin-coated samples. In the same manner, the aluminum ions were carefully investigated, and the results show that the intensities of the hydroxide ions are lower on the heated samples than on the air-dried samples, while the oxide ions present equivalent or even higher intensities on the heated samples than on the air-dried samples. Again, the observation was made assuming that the reaction happens with the free-hydroxyl groups of the metal. The proposed mechanism makes the oxygen of the amide functional group react with the free-hydroxyl groups of the metal, by creating a C−O−Al bond and an imine bond (C═N) and releasing water (see Figure 16).

## 4. MATERIALS AND METHODS

In order to achieve the objectives of this study, two types of samples have been prepared: spin-coated and dip-coated samples (see Figure 17).

To prepare spin-coated samples (Figure 17a), aluminum surfaces were first mirror polished then ethanol cleaned, permitting the deposition of a thin and homogeneous polyamide-6.6 layer by spin-coating. Three of these samples were then treated by laser welding. The welded and non-welded samples were then immersed in a 2,2,2-trifluoroethanol bath, to remove the deposited polymer layer and access the molecules bound to the metal at the interface. Three different zones were analyzed: the reference, the out of weld, and the weld. The reference was obtained with the remaining three non-welded samples. The out of weld and the weld were taken on the same samples, and these two different zones are simply distinguished by observing where the laser welding had a visible effect on the polymer layer and the zone where it did not.

The dip-coated samples (or "model samples") were essentially designed to emphasize the reaction mechanism. Therefore, a molecule composed only of the chemically reactive part of the polymer (the amide functional group) and easily processable for dip-coating was chosen: *N*-methylformamide, which is liquid at room temperature. The aluminum surfaces were simply cleaned with ethanol and then underwent $UV/O_3$ cleaning. They were then dipped in the pure compound. After, three of them were set to air dry and three others were heated on a hot plate at 150 °C. The latter temperature is below the boiling point of *N*-methylformamide at 183 °C; thereby, the desorption rate of the molecule during the heating is reduced. This temperature was chosen below the decomposition temperature of the molecule, but it is high enough to initiate reactions between the molecule and the aluminum surface.

**4.1. Materials.** A high purity (99.999%) aluminum plate was purchased from Goodfellow with a thickness of 1 mm. The plate was cut into pieces of 2 x 2 $cm^2$. Polyamide-6.6 pellets as well as *N*-methylformamide at 99% were purchased from Sigma-Aldrich and used as received. 2,2,2-Trifluoroethanol at 99+% was purchased from Alfa Aesar and was used without further purification.

**4.2. Spin-Coated Samples.** *4.2.1. Mirror polishing.* The aluminum pieces were mirror polished using an EcoMet 250 pro from Buehler. The first step was to polish the plates with SiC foil of 1200 grit from Struers. Then, diamond paste DiaDuo-2 from Struers of successively 9, 3, and 1 $\mu$m were used for the fine polishing steps. The rotation speed was 120 rpm for the sample holder and 40 rpm in counterclockwise rotation for the grit plate with 22 N pressure for 5 min. The final step to polish was made using colloidal silicon of 40 nm (OP-S from Struers) with 22 N pressure, 180 rpm sample holder speed, and 40 rpm grit speed counterclockwise for 3 min.

*4.2.2. Spin-Coating.* A 1% w/w PA-6.6 solution in 2,2,2-trifluoroethanol was spin-coated on the previously polished Al pieces, using a Laurell WS-650-23B spin coater. The speed rotation was 1000 rpm for 1 min. Afterward, the samples were let to dry for 1 h on a hot plate at 37 °C.

*4.2.3. Laser Welding.* The welding was performed by a fiber laser (TruFiber 400 from TRUMPF) with a wavelength of 1070 nm. The metal surface opposite to the metal−polymer interface was irradiated (indirect welding configuration) with a laser beam spot diameter of 58 $\mu$m. The beam followed a circular spatial power modulation (wobble trajectory), with a feed speed of 40 mm/s along the "x" axis, see Figure 2. To ensure keyhole formation while avoiding polymer degradation during the process, the heat input was controlled by applying a temporal power modulation on the laser beam. The resulting


https://doi.org/10.1021/acsomega.1c04264
ACS Omega 2021, 6, 33482−33497

temperature at the interface during the welding is about 300°C,[7] just above the melting temperature of polyamide-6.6 that is 265 °C. The laser welding procedure was described in detail previously.[7,16]

*4.2.4. Dissolution.* In order to access the interface for analysis, the samples were dipped in 100 mL of 2,2,2-trifluoroethanol overnight under mechanical stirring at 150 rpm.

**4.3. Dip-Coated Samples.** The aluminum surfaces were cleaned using a UVO cleaner model N°42-220 from Jelight Company Inc. for 5 min. Three of them were put aside to be used as references. After cleaning, the other samples were dipped in pure *N*-methylformamide for an hour at ambient temperature and pressure. For drying, the samples were then separated into two series. The first one (three samples) was left to dry at room temperature overnight, and the second one (three samples) was put on a hot plate at 150 °C for an hour.

**4.4. X-ray Photoelectron Spectroscopy (XPS).** Using a K-alpha spectrometer from Thermo Fisher Scientific, with a monochromated X-ray source (Al K$\alpha$ line at 1486 eV), the survey spectra (three scans at 200 eV pass energy) were acquired along with the high-resolution spectra of C 1s, O 1s, Al 2p, and N 1s (20 scans at 20 eV pass energy). The spectra were analyzed using the Avantage software. The C−C/C−H bond was set to 284.8 eV for energy scale calibration.

For the spin-coated samples, three reference and three welded samples were analyzed, with three analysis points for each zone (reference, out of weld, and weld), giving a total of nine measurement points per zone. For the dip-coated samples, three reference samples (description above in section 4.3), three air-dried samples, and three heated samples were analyzed each time with three measurement points, giving a total of nine measurement points per sample type.

The survey spectra were analyzed using the automatic tool of the Avantage software and then checked manually, to calculate the atomic percentages. The high-resolution spectra were interpreted by adding as few peaks as possible in order to fit the data and provide satisfying interpretation. The peak width was set to be equivalent to that of C−C/C−H with a tolerance of 0.2 eV.

**4.5. Time-of-Flight Secondary Ion Mass Spectrometry (ToF-SIMS).** The mass spectra were acquired using a ToF-SIMS IV from IONTOF in static mode and both positive and negative ion modes, using a pulsed $Bi_3^+$ ion beam set at 25 keV at an incidence angle of 45° to the normal, with a raster size of 200 × 200 $\mu m^2$ and 60 s acquisition time with a current of 0.37 pA. The extraction voltage was set to 2 kV.

For the spin-coated samples, three reference and three welded samples were analyzed, with three analysis points for each zone (reference, out of weld, and weld) in each ion polarity, for a total of 54 spectra. The same calibration ion list (in positive mode: $CH_3^+$, $Mg^+$, $AlH^+$, $Ca^+$, $C_2H_3O^+$, $CH_2NO^+$, $CH_4OAl^+$, and $C_5H_{12}N_3^+$, and in negative mode: $C^-$, $CH^-$, $C_2^-$, $C_2HO^-$, $AlO^-$, $AlO_2^-$, $C_2H_3O_2^-$, $C_5^-$, and $C_6^-$) and the same analysis peak list were used for all spectra. Large area images (in stitching mode) of 1500 × 1500 $\mu m^2$ have also been acquired under the same conditions.

For the model samples, three samples of each type (reference, air dried, and heat drying) were analyzed with three measurement points for each ion polarity for a total of 54 spectra. The same calibration ion list (in positive mode: $CH_3^+$, $CH_2N^+$, $C_3H_3^+$, $AlOH^+$, $C_4H_7^+$, $AlO_2H^+$, and $AlO_2H_2^+$, and in negative mode: $C^-$, $CH^-$, $C_2^-$, $Al^-$, $Cl^-$, $AlO^-$, $C_2H_3O^-$, $C_2H_2O_2^-$, and $AlO_2^-$) as well as the same analysis peak list were applied to all spectra.

For the spectra interpretation, peaks related to the aluminum were selected, as well as peaks related to the polyamide-6.6 or *N*-methylformamide. Classical contaminations in the SIMS spectra were also investigated. At last, peaks related to hybrid ions were identified by looking at the families of these hybrid ions ($C_xH_yAl_z^{-/+}$, $C_xH_yN_zAl_w^{-/+}$, $C_xH_yO_zAl_k^{-/+}$, and $C_xH_yN_zO_wAl_u^{-/+}$) in a systematic manner. The peak lists of both sample types and for both polarities can be found in the Supporting Information. To allow a good comparison between the different spectra, their intensities were normalized to the total intensities of the spectra. The intensities of the different ions were compared using histograms; some of them are displayed in the Results and Discussion. The main bars represent the average intensity of the corresponding ion in the zone or sample, while the error bars represent the standard deviation of the intensity.

## ■ ASSOCIATED CONTENT

### Supporting Information

The Supporting Information is available free of charge at https://pubs.acs.org/doi/10.1021/acsomega.1c04264.

XPS survey spectra of the different samples; XPS survey, C 1s, O 1s, and N 1s spectra of polyamide-6.6; the ToF-SIMS spectra from 0 to 200 *m*/*z* for the different samples in both positive and negative modes; the peak lists used for all samples in both positive and negative modes; and histograms of the normalized intensity of hybrid and metallic ions (PDF)

## ■ AUTHOR INFORMATION


### Corresponding Author

**Laurent Houssiau** − *LISE, Namur Institute for Structured Materials (NISM), Université de Namur, 61 5000 Namur, Belgium;* orcid.org/0000-0003-4923-5698; Email: laurent.houssiau@unamur.be

### Authors

**Pierre Hirchenhahn** − *LISE, Namur Institute for Structured Materials (NISM), Université de Namur, 61 5000 Namur, Belgium;* orcid.org/0000-0002-8476-5785

**Adham Al-Sayyad** − *Research Unit in Engineering Science, Université de Luxembourg, L-1359 Luxembourg-Kirchberg, Luxembourg*

**Julien Bardon** − *Luxembourg Institute of Science and Technology, L-4362 Esch-sur-Alzette, Luxembourg*

**Peter Plapper** − *Research Unit in Engineering Science, Université de Luxembourg, L-1359 Luxembourg-Kirchberg, Luxembourg*

Complete contact information is available at: https://pubs.acs.org/10.1021/acsomega.1c04264


### Notes

The authors declare no competing financial interest.

## ■ ACKNOWLEDGMENTS

The work was funded by the DGO6 of the Walloon region and the FNR of Luxembourg through the M-Era.Net project entitled LaserSTAMP. All the XPS and ToF-SIMS experiments were performed using the equipment available at the SIAM platform at the University of Namur.

## REFERENCES


(1) Speck, J. A. *Mechanical Fastening, Joining, and Assembly*; second, CRC Press, 2015.
(2) Skeist, I. *Handbook of Adhesives*; Third edit.; Chapman & Hall: New York, 1990.
(3) Amancio-Filho, S. T.; Dos Santos, J. F. Joining of Polymers and Polymer-Metal Hybrid Structures: Recent Developments and Trends. *Polym. Eng. Sci.* **2009**, *49*, 1461−1476.
(4) da Costa, A. P.; Botelho, E. C.; Costa, M. L.; Narita, N. E.; Tarpani, J. R. A Review of Welding Technologies for Thermoplastic Composites in Aerospace Applications. *J. Aerosp. Technol. Manag.* **2012**, *4*, 255−266.
(5) Yousefpour, A.; Hojjati, M.; Immarigeon, J.-P. Fusion Bonding/Welding of Thermoplastic Composites. *J. Thermoplast. Compos. Mater.* **2004**, *17*, 303−341.
(6) Al-Sayyad, A.; Bardon, J.; Hirchenhahn, P.; Santos, K.; Houssiau, L.; Plapper, P. Aluminum Pretreatment by a Laser Ablation Process: Influence of Processing Parameters on the Joint Strength of Laser Welded Aluminum - Polyamide Assemblies. *Procedia CIRP* **2018**, *74*, 495−499.
(7) Lamberti, C.; Solchenbach, T.; Plapper, P.; Possart, W. Laser Assisted Joining of Hybrid Polyamide-Aluminum Structures. *Phys. Procedia* **2014**, *56*, 845−853.
(8) Arai, S.; Kawahito, Y.; Katayama, S. Effect of Surface Modification on Laser Direct Joining of Cyclic Olefin Polymer and Stainless Steel. *Mater. Des.* **2014**, *59*, 448−453.
(9) Sun, Z.; Ion, J. C. Laser Welding of Dissimilar Metal Combinations. *J. Mater. Sci.* **1995**, *30*, 4205−4214.
(10) Katayama, S.; Kawahito, Y. Laser Direct Joining of Metal and Plastic. *Scr. Mater.* **2008**, *59*, 1247−1250.
(11) Tamrin, K. F.; Nukman, Y.; Zakariyah, S. S. Laser Lap Joining of Dissimilar Materials: A Review of Factors Affecting Joint Strength. *Mater. Manuf. Processes* **2013**, *28*, 857−871.
(12) Holtkamp, J.; Roesner, A.; Gillner, A. Advances in Hybrid Laser Joining. *Int. J. Adv. Manuf. Technol.* **2010**, *47*, 923−930.
(13) Katayama, S.; Kawahito, Y.; Mizutani, M. Latest Progress in Performance and Understanding of Laser Welding. *Phys. Procedia* **2012**, *39*, 8−16.
(14) Schricker, K.; Stambke, M.; Bergmann, J. P. Experimental Investigations and Modeling of the Melting Layer in Polymer-Metal Hybrid Structures. *Weld. World* **2015**, *59*, 407−412.
(15) Schricker, K.; Diller, S.; Bergmann, J. P. Bubble Formation in Thermal Joining of Plastics with Metals. *Procedia CIRP* **2018**, *74*, 518−523.
(16) Al-Sayyad, A.; Bardon, J.; Hirchenhahn, P.; Vaudémont, R.; Houssiau, L.; Plapper, P. Influence of Aluminum Laser Ablation on Interfacial Thermal Transfer and Joint Quality of Laser Welded Aluminum-Polyamide Assemblies. *Coatings* **2019**, *9*, 768.
(17) Hirchenhahn, P.; Al-Sayyad, A.; Bardon, J.; Felten, A.; Plapper, P.; Houssiau, L. Highlighting Chemical Bonding between Nylon-6.6 and the Native Oxide from an Aluminum Sheet Assembled by Laser Welding. *ACS Appl. Polym. Mater.* **2020**, *2*, 2517−2527.
(18) Swift, P. Adventitious Carbon—the Panacea for Energy Referencing? *Surf. Interface Anal.* **1982**, *4*, 47−51.
(19) Miller, D. J.; Biesinger, M. C.; McIntyre, N. S. Interactions of CO2 and CO at Fractional Atmosphere Pressures with Iron and Iron Oxide Surfaces: One Possible Mechanism for Surface Contamination? *Surf. Interface Anal.* **2002**, *33*, 299−305.
(20) Piao, H.; McIntyre, N. S. Adventitious Carbon Growth on Aluminium and Gold-Aluminium Alloy Surfaces. *Surf. Interface Anal.* **2002**, *33*, 591−594.
(21) Barr, T. L.; Seal, S. Nature of the Use of Adventitious Carbon as a Binding Energy Standard. *J. Vac. Sci. Technol. A Vacuum, Surfaces, Film.* **1995**, *13*, 1239−1246.
(22) Beamson, G.; Briggs, D. *High Resolution XPS of Organic Polymers, the Scienta ESCA300 Database.*; John Wiley & Sons, Ltd., 1992.
(23) Wagner, C. D.; Riggs, W. M.; Davis, L. E.; Moulder, J. F.; Muilenberg, G. E. *Handbook of X-Ray Photoelectron Spectroscopy : A Reference Book of Standard Spectra for Identification and Interpretation of XPS Data - Catalog - UW-Madison Libraries*; Physical Electronics, 1995.
(24) Mohtasebi, A.; Chowdhury, T.; Hsu, L. H. H.; Biesinger, M. C.; Kruse, P. Interfacial Charge Transfer between Phenyl-Capped Aniline Tetramer Films and Iron Oxide Surfaces. *J. Phys. Chem. C* **2016**, *120*, 29248−29263.
(25) Alexander, M. R.; Thompson, G. E.; Beamson, G. Characterization of the Oxide/Hydroxide Surface of Aluminum Using X-Ray Photoelectron Spectroscopy: A Procedure for Curve Fitting the O 1s Core Level. *Surf. Interface Anal.* **2000**, *29*, 468−477.
(26) Alexander, M. R.; Beamson, G.; Blomfield, C. J.; Leggett, G.; Duc, T. M. Interaction of Carboxylic Acids with the Oxyhydroxide Surface of Aluminium: Poly(Acrylic Acid), Acetic Acid and Propionic Acid on Pseudoboehmite. *J. Electron Spectros. Relat. Phenomena* **2001**, *121*, 19−32.
(27) Baldan, A. Adhesion Phenomena in Bonded Joints. *Int. J. Adhes. Adhes.* **2012**, *38*, 95−116.
(28) Rajan, T. P. D.; Pillai, R. M.; Pai, B. C. Reinforcement Coatings and Interfaces in Aluminium Metal Matrix Composites. *J. Mater. Sci.* **1998**, *33*, 3491−3503.
(29) Pippel, E.; Woltersdorf, J.; Doktor, M.; Blucher, J.; Degischer, H. P. Interlayer Structure of Carbon Fibre Reinforced Aluminum Wires. *J. Mater. Sci.* **2000**, *35*, 2279−2289.
(30) Blucher, J. T.; Dobranszky, J.; Narusawa, U. Aluminium Double Composite Structures Reinforced with Composite Wires. *Mater. Sci. Eng., A* **2004**, *387-389*, 867−872.
(31) Etter, T.; Schulz, P.; Weber, M.; Metz, J.; Wimmler, M.; Löffler, J. F.; Uggowitzer, P. J. Aluminium Carbide Formation in Interpenetrating Graphite/Aluminium Composites. *Mater. Sci. Eng., A* **2007**, *448*, 1−6.
(32) Yang, M.; Scott, V. D. Carbide Formation in a Carbon Fibre Reinforced Aluminium Composite. *Carbon N. Y.* **1991**, *29*, 877−879.
(33) Esawi, A. M. K.; Morsi, K.; Sayed, A.; Taher, M.; Lanka, S. Effect of Carbon Nanotube (CNT) Content on the Mechanical Properties of CNT-Reinforced Aluminium Composites. *Compos. Sci. Technol.* **2010**, *70*, 2237−2241.
(34) Li, S. H.; Chao, C. G. Effects of Carbon Fiber/Al Interface on Mechanical Properties of Carbon-Fiber-Reinforced Aluminum-Matrix Composites. *Metall. Mater. Trans. A Phys. Metall. Mater. Sci.* **2004**, *35 A*, 2153−2160.
(35) Kuda-Malwathumullage, C. P. S.; Small, G. Determination of Moisture Content of Polyamide 66 Directly from Combination Region Near-Infrared Spectra. *J. Appl. Polym. Sci.* **2014**, *131*, 40645.
(36) Malengreau, F.; Hautier, V.; Vermeersch, M.; Sporken, R.; Caudano, R. Chemical Interactions at the Interface between Aluminium Nitride and Iron Oxide Determined by XPS. *Surf. Sci.* **1995**, *330*, 75−85.
(37) Bertóti, I. Characterization of Nitride Coatings by XPS. *Surf. Coatings Technol.* **2002**, *151−152*, 194−203.
(38) Rosenberger, L.; Baird, R.; McCullen, E.; Auner, G.; Shreve, G. XPS Analysis of Aluminum Nitride Films Deposited by Plasma Source Molecular Beam Epitaxy. *Surf. Interface Anal.* **2008**, *40*, 1254−1261.
(39) Bauer, J.; Biste, L.; Bolze, D. Optical Properties of Aluminium Nitride Prepared by Chemical and Plasmachemical Vapour Deposition. *Phys. status solidi* **1977**, *39*, 173−181.
(40) Okano, H.; Tanaka, N.; Takahashi, Y.; Tanaka, T.; Shibata, K.; Nakano, S. Preparation of Aluminum Nitride Thin Films by Reactive Sputtering and Their Applications to GHz-Band Surface Acoustic Wave Devices. *Appl. Phys. Lett.* **1994**, *64*, 166−168.
(41) Tsuchida, T.; Hasegawa, T.; Kitagawa, T.; Inagaki, M. Aluminium Nitride Synthesis in Air from Aluminium and Graphite Mixtures Mechanically Activated. *J. Eur. Ceram. Soc.* **1997**, *17*, 1793−1795.
(42) Carlos Rojo, J.; Slack, G. A.; Morgan, K.; Raghothamachar, B.; Dudley, M.; Schowalter, L. J. Report on the Growth of Bulk Aluminum Nitride and Subsequent Substrate Preparation. *J. Cryst. Growth* **2001**, *231*, 317−321.



https://doi.org/10.1021/acsomega.1c04264
*ACS Omega* 2021, 6, 33482−33497

(43) Yu, C. H.; Huang, C. H.; Tan, C. S. A Review of $CO_2$ Capture by Absorption and Adsorption. *Aerosol Air Qual. Res.* **2012**, *12*, 745−769.
(44) Lin, Z.; Meyer, H. M.; Weaver, J. H.; Anderson, S. G.; Atanasoska, L. Aluminum/Polyimide Interface Formation: An X-ray Photoelectron Spectroscopy Study of Selective Chemical Bonding. *J. Vac. Sci. Technol. A Vacuum, Surfaces, Film.* **2002**, *5*, 3325−3333.
(45) Bartha, J. W.; Hahn, P. O.; LeGoues, F.; Ho, P. S. Photoemission Spectroscopy Study of Aluminum−Polyimide Interface. *J. Vac. Sci. Technol. A Vacuum, Surfaces, Film.* **2002**, *3*, 1390−1393.
(46) Zhu, H.; Chen, Z.; Sheng, Y.; Luong Thi, T. T. Flaky Polyacrylic Acid/Aluminium Composite Particles Prepared Using in-Situ Polymerization. *Dyes Pigm.* **2010**, *86*, 155−160.
(47) Vermöhlen, K.; Lewandowski, H.; Narres, H. D.; Koglin, E. Adsorption of Polyacrylic Acid on Aluminium Oxide: DRIFT Spectroscopy and Ab Initio Calculations. *Colloids Surfaces A Physicochem. Eng. Asp.* **2000**, *170*, 181−189.
(48) Pletincx, S.; Marcoen, K.; Trotochaud, L.; Fockaert, L. L.; Mol, J. M. C.; Head, A. R.; Karslioğlu, O.; Bluhm, H.; Terryn, H.; Hauffman, T. Unravelling the Chemical Influence of Water on the PMMA/Aluminum Oxide Hybrid Interface in Situ. *Sci. Rep.* **2017**, *7*, 1−11.
(49) de Gennes, P. G. Reptation of a Polymer Chain in the Presence of Fixed Obstacles. *J. Chem. Phys.* **1971**, *55*, 572−579.
(50) Strohmeier, B. R. An Esca Method for Determining the Oxide Thickness on Aluminum-Alloys. *Surf. Interface Anal.* **1990**, *15*, 51−56.
(51) Abel, M. L.; Rattana, A.; Watts, J. F. Interaction of γ-Glycidoxypropyltrimethoxysilane with Oxidized Aluminum Substrates: The Effect of Drying Temperature. *J. Adhes.* **2000**, *73*, 313−340.
(52) Rattana, A.; Hermes, J. D.; Abel, M. L.; Watts, J. F. The Interaction of a Commercial Dry Film Adhesive with Aluminium and Organosilane Treated Aluminium Surfaces: A Study by XPS and ToF-SIMS. *Int. J. Adhes. Adhes.* **2002**, *22*, 205−218.
(53) Watts, J. F.; Rattana, A.; Abel, M. L. Interfacial Chemistry of Adhesives on Hydrated Aluminium and Hydrated Aluminium Treated with an Organosilane. *Surf. Interface Anal.* **2004**, *36*, 1449−1468.
(54) Van den Brand, J.; Sloof, W. G.; Terryn, H.; De Wit, J. H. W. Correlation between Hydroxyl Fraction and O/Al Atomic Ratio as Determined from XPS Spectra of Aluminium Oxide Layers. *Surf. Interface Anal.* **2004**, *36*, 81−88.
(55) Van den Brand, J.; Snijders, P. C.; Sloof, W. G.; Terryn, H.; De Wit, J. H. W. Acid-Base Characterization of Aluminum Oxide Surfaces with XPS. *J. Phys. Chem. B* **2004**, *108*, 6017−6024.
(56) Abel, M. L.; Joannic, R.; Fayos, M.; Lafontaine, E.; Shaw, S. J.; Watts, J. F. Effect of Solvent Nature on the Interaction of γ-Glycidoxy Propyl Trimethoxy Silane on Oxidised Aluminium Surface: A Study by Solution Chemistry and Surface Analysis. *Int. J. Adhes. Adhes.* **2006**, *26*, 16−27.
(57) Shimizu, K.; Abel, M. L.; Watts, J. F. Evaluation of the Interaction and Adsorption of γ-Glycidoxy Propyl Trimethoxy Silane with Grit-Blasted Aluminium: A ToF-SIMS and XPS Study. *J. Adhes.* **2008**, *84*, 725−741.
(58) Abrahami, S. T.; Hauffman, T.; De Kok, J. M. M.; Mol, J. M. C.; Terryn, H. Effect of Anodic Aluminum Oxide Chemistry on Adhesive Bonding of Epoxy. *J. Phys. Chem. C* **2016**, *120*, 19670−19677.
(59) Fockaert, L. I.; Taheri, P.; Abrahami, S. T.; Boelen, B.; Terryn, H.; Mol, J. M. C. Zirconium-Based Conversion Film Formation on Zinc, Aluminium and Magnesium Oxides and Their Interactions with Functionalized Molecules. *Appl. Surf. Sci.* **2017**, *423*, 817−828.
(60) Pletincx, S.; Mol, J. M. C.; Terryn, H.; Hubin, A.; Hauffman, T. An in Situ Spectro-Electrochemical Monitoring of Aqueous Effects on Polymer/Metal Oxide Interfaces. *J. Electroanal. Chem.* **2019**, *848*, 113311.


https://doi.org/10.1021/acsomega.1c04264
*ACS Omega* 2021, 6, 33482−33497